Proceedings of IMECE2006
2006 ASME International Mechanical Engineering Congress and Exposition
November 5-10, 2006, Chicago, Illinois, USA

IMECE2006-13693

A SISO, MULTI-ANALYTE SENSOR BASED ON A COUPLED MICRORESONATOR ARRAY

Jeffrey F. Rhoads*
Department of Mechanical Engineering
Michigan State University
East Lansing, Michigan 48824
Email: rhoadsje@msu.edu

Barry E. DeMartini
Department of Mechanical Engineering
University of California, Santa Barbara
Santa Barbara, California 93106
Email: baredog@umail.ucsb.edu

Steven W. Shaw
Department of Mechanical Engineering
Michigan State University
East Lansing, Michigan 48824
Email: shawsw@msu.edu

Kimberly L. Turner
Department of Mechanical Engineering
University of California, Santa Barbara
Santa Barbara, California 93106
Email: turner@engineering.ucsb.edu

ABSTRACT

This work details a preliminary analytical and experimental investigation of a new class of resonant, single input - single output (SISO) microsensors, which are capable of detecting multiple analytes. The key feature of these sensors is that they exploit vibration localization in a set of N microbeams, coupled indirectly through a common shuttle mass, to allow for the detection of N distinct resonance shifts (induced by the presence of up to N distinct analytes) using solely the shuttle mass' response. The work includes a brief overview of the proposed sensor design, the formulation and subsequent analysis of a representative lumped-mass model of the sensor, and details of a recently-completed simulated mass detection experiment, which verified the feasibility of the proposed sensor design. Where appropriate, practical design issues, essential to sensor development, are described.

INTRODUCTION

Chemical, biological, and mass sensors based on resonant microsystems have been proposed for use in a wide variety of applications ranging from environmental monitoring to medical diagnostics [1–14]. The principal interest in such devices stems not only from their broad applicability, but also the reduction in size and power and the potential for improved sensitivity they offer. Typically, resonant microsensors exploit induced resonance shifts for sensing. As these shifts arise from mass or stiffness changes in the oscillator, caused by adsorption, desorption, or local stress stiffening at the oscillator's surface, they can be used to identify the presence of a target analyte [15–17]. Unfortunately, due to the practical limitations of surface science and the fact that the oscillators typically feature a single dominant degree-of-freedom (SDOF), only a lone analyte or group of analytes can generally be detected through this approach. Arrays of isolated oscillators, individually functionalized to detect a specific analyte, can be used to broaden detection capabilities (see, for example, [16]), but the inherent complexity of such arrays (arising from increased hardware and signal processing requirements) limits their utility.

This work presents a novel sensor architecture that realizes the detection capabilities of a resonant sensor array in the context of a single input - single output (SISO) system. This is accomplished by mechanically coupling an array of frequency-mistuned microbeam resonators, each functionalized to a given

*Address all correspondence to this author.

Copyright © 2006 by ASME

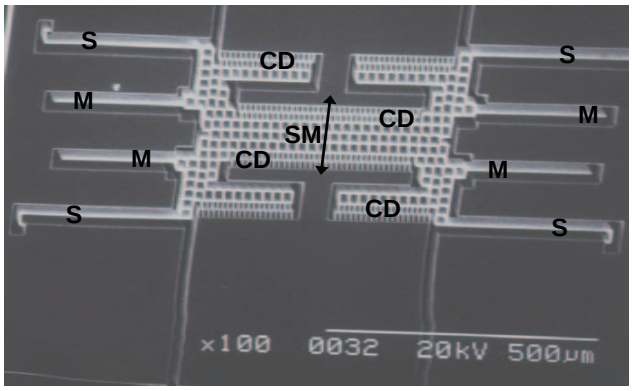

Figure 1. A SCANNING ELECTRON MICROGRAPH OF A TRANSLATIONAL, SISO, MULTI-ANALYTE SENSOR. NOTE THAT THE DEVICE'S SHUTTLE MASS IS LABELED SM, THE INDIVIDUAL MICROBEAM OSCILLATORS M, THE ELECTROSTATIC COMB DRIVES CD, AND THE FOLDED BEAM FLEXURES S [18]. ALSO NOTE THAT THE ARROW INDICATES THE PRINCIPAL DIRECTION OF MOTION.

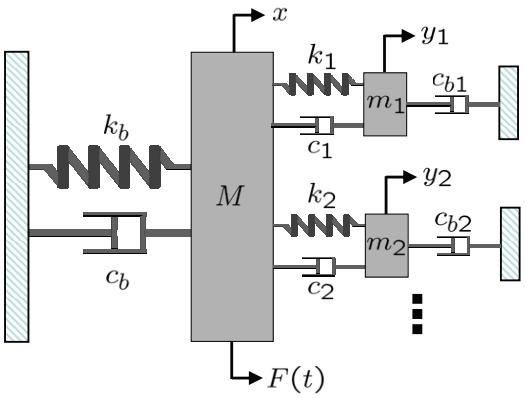

Figure 2. A MASS-SPRING-DASHPOT ANALOG OF THE SENSOR DEPICTED IN FIG. 1 [18]. NOTE THAT THE LARGER MASS M IS USED TO REPRESENT THE SENSOR'S SHUTTLE MASS AND THE COMPARATIVELY SMALLER MASSES m_i REPRESENT THE MICROBEAM OSCILLATORS.

analyte or group of analytes, to a common shuttle mass, which is used for both sensing and actuation (see Fig. 1). The principal benefit of this approach is that, given vibration localization in the set of mistuned oscillators, the shuttle mass itself can be used to track resonance shifts in the individual microbeams [18]. Accordingly, a single, SISO device proves sufficient for the detection of multiple analytes.

This work details a joint analytical and experimental investigation of the innovative sensor design described above. In particular, the work begins with a brief overview of the sensor's topology and the systematic formulation of a representative lumped-mass model amenable to analysis. Following this, pertinent features of a desirable form of the sensor's frequency response are discussed and experimental results, obtained from a simulated mass detection event, are detailed. The work concludes with a brief look at the sensor's performance metrics and an outline of future work. It should be noted that, where appropriate, practical design issues essential to sensor development are described.

SYSTEM MODELING

Though a number of topologically equivalent geometries can be (and have been) developed based on the sensing principles discussed herein, the translational design depicted in Fig. 1 was selected as the principal focus of this work. This relatively simple sensor geometry consists of a shuttle mass (SM) that is suspended above the substrate by four folded beam flexures (S) and driven by interdigitated electrostatic comb drives (CD). Attached to this shuttle are four microbeam oscillators (M) each with slight frequency mistuning, as realized through small length variations, to ensure ample separation of the coupled system's natural frequencies – a necessary precursor for localization, as subsequently described.

The relevant response characteristics of the device shown in Fig. 1 can be described through the use of the simple linear lumped-mass model shown in Fig. 2. Here the N microbeam oscillators are represented by the smaller masses, m_1, m_2, etc., and the comparatively larger shuttle mass is represented by M. It is important to note that while topologies such as that shown in Fig. 2 are believed to be novel in the sensors community, they have garnered attention in other contexts, namely noise control and vibration suppression [19–21]. Unfortunately, given the stark contrast between these applications and that considered here, as well as the requisite form of each of the systems' frequency responses, the results of the previous works are not directly applicable to the present study.

The equations of motion governing the system depicted in Fig. 2 are given by

$$M\ddot{x}+\sum_i m_i\left(\ddot{x}+\ddot{z}_i\right)+\sum_i c_{bi}\left(\dot{x}+\dot{z}_i\right)+c_b\dot{x}+k_b x=F(t), \qquad (1)$$

$$m_i\left(\ddot{x}+\ddot{z}_i\right)+c_{bi}\left(\dot{x}+\dot{z}_i\right)+c_i\dot{z}+k_i z=0, \qquad i=1,\ldots,N \qquad (2)$$

where z_i is the relative displacement of the ith subsystem, given by

$$z_i=y_i-x, \qquad i=1,\ldots,N, \qquad (3)$$

c_b, c_i and c_{bi} represent linear damping coefficients arising from intrinsic and extrinsic dissipation, and $F(t)$ represents the electrostatic force produced by the interdigitated comb drives [18].

Copyright © 2006 by ASME

Assuming ample device thickness (approximately 10 μm or larger) and a harmonic voltage excitation of the form

$$V(t) = V_A \cos \omega t, \tag{4}$$

the electrostatic force, $F(t)$, can be approximated by

$$F(t) = \frac{\varepsilon_0 n h V^2(t)}{g} = \frac{\varepsilon_0 n h V_A^2}{2g}\left(1+\cos 2\omega t\right) = F_0\left(1+\cos 2\omega t\right), \tag{5}$$

where ε_0 represents the free space permittivity, n the number of comb fingers on the electrostatic comb drive, g the gap between adjacent comb fingers, and h the device thickness. Nondimensionalizing the resulting equations of motion and redefining the dynamic variables x and z by translation according to

$$\hat{x} = x - \bar{x} = x - \frac{F_0}{k_b}, \qquad \hat{z} = z \tag{6}$$

to eliminate the explicit DC forcing term (which is dependent on V_A) results in a new set of governing equations given by

$$\begin{aligned} &u'' + 2\zeta_b \Lambda u' + \Lambda^2 u \\ &\quad = \Gamma \cos \Omega\tau - \sum_i \hat{m}_i\left(u'' + v_i''\right) - \sum_i 2\zeta_{bi}\Upsilon_i \hat{m}_i\left(u' + v_i'\right) \end{aligned} \tag{7}$$

$$\begin{aligned} &\hat{m}_i\left(u'' + v_i''\right) + 2\zeta_i \Upsilon_i \hat{m}_i v_i' + \hat{m}_i \Upsilon_i^2 v_i \\ &\quad = -2\zeta_{bi}\Upsilon_i \hat{m}_i\left(u' + v_i'\right) \qquad i = 1,\ldots,N \end{aligned} \tag{8}$$

with system parameters defined as in Tab. 1. For the sake of analysis, these equations can be compiled into a standard matrix form given by

$$MX'' + CX' + KX = \Phi(\tau), \tag{9}$$

where X represents the compiled state vector, M the effective mass matrix (which incorporates inertial coupling terms), C the effective damping matrix (which incorporates dissipative coupling terms), K the effective stiffness matrix, and $\Phi(\tau)$ the effective forcing vector, which is sparse except for the first element. From this matrix equation, the system's response can be easily determined through a variety of standard techniques, including that utilized for the present work – the impedance approach detailed in [22].

Table 1. NONDIMENSIONAL PARAMETER DEFINITIONS. NOTE THAT x_0 AND ω_0 REPRESENT A CHARACTERISTIC LENGTH AND FREQUENCY OF THE SYSTEM, RESPECTIVELY.

Parameter	Description
$\tau = \omega_0 t$	Nondimensional Time
$\Omega = \frac{2\omega}{\omega_0}$	Nondimensional Excitation Frequency
$(\bullet)' = \frac{d(\bullet)}{d\tau}$	New Derivative Operator
$u = \frac{\hat{x}}{x_0}$, $v_i = \frac{\hat{z}_i}{x_0}$	Nondimensional Displacements
$\hat{m}_i = \frac{m_i}{M}$	Inertia Ratio
$\Lambda = \frac{\omega_b}{\omega_0} = \frac{1}{\omega_0}\sqrt{\frac{k_b}{M}}$	Frequency Ratio
$\Upsilon_i = \frac{\omega_i}{\omega_0} = \frac{1}{\omega_0}\sqrt{\frac{k_i}{m_i}}$	Frequency Ratio
$\zeta_b = \frac{c_b}{2\sqrt{k_b M}}$	Damping Ratio
$\zeta_i = \frac{c_i}{2\sqrt{k_i m_i}}$	Damping Ratio
$\zeta_{bi} = \frac{c_{bi}}{2\sqrt{k_i m_i}}$	Pseudo-Damping Ratio
$\Gamma = \frac{F_0}{M x_0 \omega_0^2}$	Nondimensional Excitation Amplitude

FREQUENCY RESPONSE CHARACTERISTICS

Because of the large number of parameters $(4N+4)$ present in Eq. 9, a number of qualitatively distinct frequency responses can be realized using the sensor topology detailed in Fig. 2. Unfortunately, most of these responses are poorly suited for sensing. One form of the system frequency response, recovered using techniques similar to those outlined in [22], which is amenable to sensing is shown in Fig. 3 [18]. Several features of this response are worth noting. First, the response includes a low-frequency resonance (1), which approximately occurs at the resonant frequency

$$\Omega_0 \approx \frac{1}{\omega_0}\sqrt{\frac{k_b}{M + \sum_i^N m_i}}, \tag{10}$$

corresponding to a bulk, in-plane mode where essentially all of the microbeams are moving together with the shuttle mass as a lumped mass. Additionally, the response includes four comparatively higher frequency resonances: (A), (B), (C), and (D). These resonances occur at frequencies slightly greater than Υ_i and correspond to in-plane modes where the system's energy is largely localized in, or confined to, a single microbeam (as confirmed by noting the comparatively larger resonant amplitudes). As these higher frequency resonances (corresponding to the localized modes) induce a measurable resonance in the response of

Copyright © 2006 by ASME

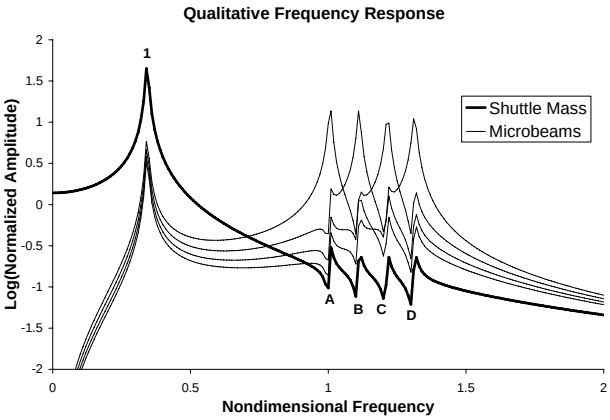

Figure 3. A DESIRABLE FORM OF THE FREQUENCY RESPONSE FOR A REPRESENTATIVE SENSOR DESIGN. NOTE THAT THE LABELED RESONANCES CORRESPOND TO THE FOLLOWING MODES: (1) A TRANSLATIONAL IN-PLANE MODE, (A, B, C, AND D) MODES WHERE ENERGY IS LOCALIZED IN ONE OF THE SYSTEM'S MICROBEAMS.

.

the shuttle mass M, resonance shifts induced by chemomechanical processes on any of the microbeams can be detected using solely the shuttle mass' response. Accordingly, sweeping the excitation frequency of the system Ω through a frequency domain that includes Υ_1, ..., Υ_N allows for the detection of up to N distinct analytes, providing proper functionalization.

Given the large number of qualitatively distinct frequency responses that can be obtained for the system depicted in Fig. 2, it is important to note how responses similar to that shown in Fig. 3, which are well suited for resonant mass sensing, can be recovered through the careful selection of system parameters. To this end, details on the selection of system inertia ratios ($\hat{m}_i$), system frequency ratios (Υ_i/Λ), and the amplitude of the AC voltage excitation applied to the electrostatic comb drives (V_A), which manifests itself in Γ, are detailed here.

To ensure ample separation between resonances (A), (B), (C), and (D), as well as all other resonances corresponding to both in-plane and out-of-plane modes, the frequency ratios (Υ_i/Λ) must be carefully selected. Specifying Υ_i/Λ too close to unity leads to little or no separation between the low-frequency resonance (1) and resonances (A)-(D). This results in the saturation of the resonant peaks associated with the localized modes, which can hinder the detection of resonance shifts, especially in the presence of additive noise. Similar decreases in resonant amplitudes can occur if the resonances occurring at approximately Υ_i are placed too close to resonances corresponding to out-of-plane modes or higher frequency in-plane modes (neither of which are captured with the lumped-mass model detailed here, but both of which could be captured through modal analysis of the structure using finite element techniques). It should also be noted that each Υ_i/Λ value must be well separated from all other Υ_i/Λ values, as placing two resonances too close together can lead to the formation of a multi-resonance passband (i.e. the resonance peaks become indistinct), which prevents the detection of individual resonance shifts – a necessity for the SISO mass sensing methods detailed here.

Due to the presence of inertial coupling in Eq. 9, specification of the system's inertia ratios ($\hat{m}_i$) is used to control the coupling strength between the microbeams and the shuttle mass, and thus is used in conjunction with frequency ratio selection to manipulate the degree of localization in the coupled system's response [23]. For the device considered herein, strong mode localization is a prerequisite for efficient mass sensing. This can be attributed to the fact that while mass and/or stiffness changes in a single microbeam lead to shifts in all of the system's resonances, in the presence of strong mode localization these mass and/or stiffness changes induce a significantly larger shift in the resonance associated with the altered oscillator. This, providing selective surface functionalization, allows for the rapid identification of a given resonance shift's source (namely, the particular microbeam, which having undergone a chemomechanical process, has had its mass and/or stiffness altered), which may ultimately facilitate automated analyte identification.

Given the linear nature of the system detailed here, manipulation of the AC excitation voltage amplitude (V_A) is used primarily to control the relative amplitude of the shuttle mass' response. As the ability to operate in low-Q environments is an ultimate goal with this sensor, large amplitude responses, realized using a comparatively large excitation amplitude, are generally desirable. These large amplitudes, however, can lead to a nonlinear resonance structure, which proves problematic for sensing. As such, practical magnitude constraints on V_A must be adopted and accounted for in the course of design.

PRELIMINARY EXPERIMENTAL RESULTS

To validate the SISO, multi-analyte sensor concept detailed herein, the device depicted in Fig. 1 was fabricated using a standard silicon-on-insulator (SOI) process flow, which included a single lithographic step, followed by a silicon deep etch (performed using DRIE), an O_2 reactive ion etch (RIE) to remove excess polymers, and, finally, a wet hydrofluoric acid (HF) etch to undercut and release the device [24]. Mass detection was then simulated by comparing the sensor shuttle mass' frequency response before and after the deposition of a small amount of mass on the highest frequency microbeam resonator. For this preliminary experiment, actuation was provided electrostatically through the integrated comb drives and response measurements were obtained optically through single beam laser vibrometry [25]. Note that as the device vibrates in-plane in the desired mode of operation, a 45° mirror was cut into the silicon adjacent to the

Copyright © 2006 by ASME

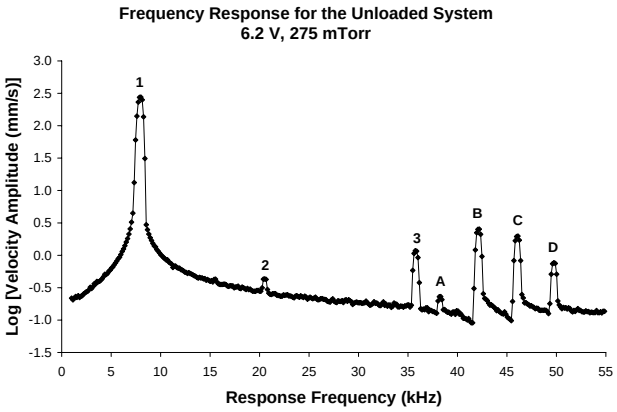

Figure 4. EXPERIMENTALLY-OBTAINED FREQUENCY RESPONSE FOR THE SENSOR DEPICTED IN FIG. 1 ACTUATED WITH A 6.2 V AC SIGNAL IN 275 mTORR PRESSURE [18]. NOTE THAT THE LABELED RESONANCES CORRESPOND TO THE FOLLOWING MODES: (1) BULK IN-PLANE MODE, (2, 3) OUT-OF-PLANE MODES, (A, B, C, AND D) MODES WHERE ENERGY IS LOCALIZED IN ONE OF THE SYSTEM'S MICROBEAMS.

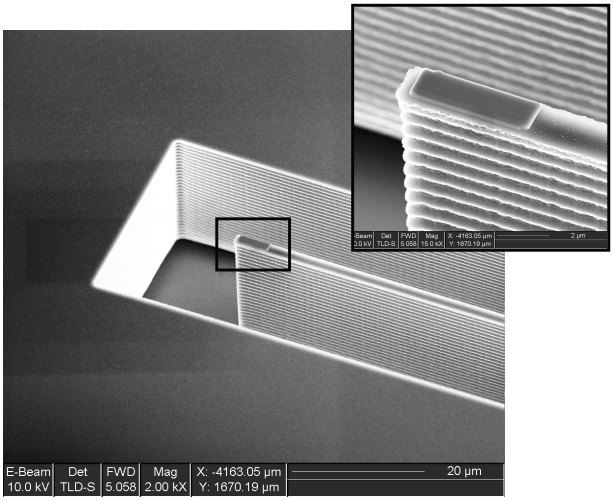

Figure 5. A SCANNING ELECTRON MICROGRAPH OF THE PLATINUM PATCH ADDED TO THE SHORTEST MICROBEAM [18]. THE INSET, WHICH WAS USED FOR MEASUREMENT PURPOSES, SHOWS A CLOSER VIEW. THE PATCH MEASURES APPROXIMATELY 1.57 x 5.10 x 0.22 μm IN SIZE AND HAS A MASS OF APPROXIMATELY 38 pg.

shuttle mass using a focused ion beam. This permitted the laser to be reflected off the mirror and onto the shuttle mass itself, thus allowing for the direct acquisition of the shuttle mass' velocity.

Figure 4 shows the frequency response acquired for the sensor depicted in Fig. 1, actuated with a 6.2 V AC signal in 275 mTorr pressure, prior to added mass deposition. As evident, the response is largely compatible with the desired form of the frequency response shown in Fig. 3. Specifically, the response includes a low frequency resonance (1) at approximately 8 kHz, which corresponds to the bulk in-plane mode; two resonances (2) and (3), not predicted by the lumped-mass model, but subsequently predicted via finite element methods, at approximately 20 and 36 kHz, which correspond to out-of-plane modes; and four resonances (A)-(D) occurring between approximately 37 kHz and 50 kHz with approximately 4 kHz spacing, which correspond to the microbeam-localized modes of the system. It should be noted that the localized nature of the latter modes has been verified visually through the use of a stroboscopic in-plane measurement system with video capture capabilities. Furthermore, it is worth noting that the proximity of resonances (3) and (A) led to an unsatisfactory reduction in the amplitude of resonance (A). Though this proved to be inconsequential in the present study, this could prove problematic in implementation, as alluded to in the previous section.

Following the acquisition of the frequency response data summarized in Fig. 4, a small platinum patch, measuring approximately 1.57 x 5.10 x 0.22 μm with an approximate mass of 38 pg, was deposited at the tip of the highest frequency microbeam (this location on the microbeam was selected to ensure the largest possible frequency shift [26]) using a focused ion beam (FIB) deposition system (see Fig. 5). The effect of this added mass is detailed in Fig. 6, which shows a close-up view of the sensor's frequency response near the four resonances corresponding to the localized microbeam modes, obtained prior to and after platinum deposition. As evident, the added mass caused shifts in each of the system's resonances, but the most pronounced shift, by far, occurred in the resonance associated with the localized mode of the highest frequency microbeam (that to which the platinum patch was added). This is verified through closer examination of the individual resonance peaks shown in Figs. 7 and 8. Specifically, it is seen that resonance (D), that associated with the localized mode of the altered microbeam, shifted by approximately 124 Hz and resonance (C), the resonance with the next largest shift, shifted by only approximately 3 Hz (it is worth noting that these values are comparable in magnitude to those predicted using both analytical and finite element methods, though parameter uncertainty does yield some discrepancy). Accordingly, due the localized nature of the sensor's response, the resonance shift associated with the mass added beam was approximately 40 times greater than that of the next largest resonance shift, a fact that could be used in implementation to identify the altered microbeam.

Copyright © 2006 by ASME

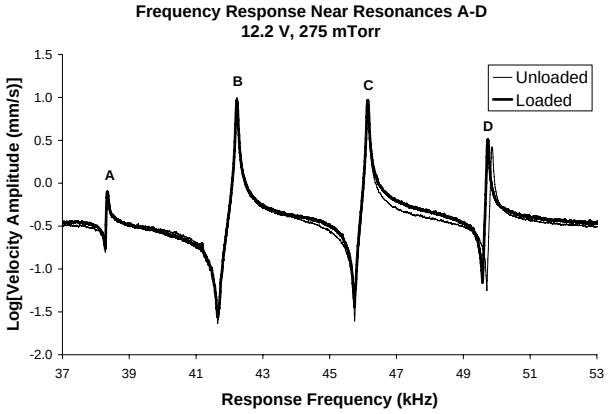

Figure 6. EXPERIMENTALLY-OBTAINED FREQUENCY RESPONSE FOR THE SENSOR DEPICTED IN FIG. 1 ACTUATED WITH A 12.2 V AC SIGNAL IN 275 mTORR PRESSURE [18]. NOTE THAT THE ADDED-MASS LOADING INTRODUCES RESONANCE SHIFTS, THE LARGEST OF WHICH OCCURS IN RESONANCE (D), WHICH CORRESPONDS TO THE LOCALIZED MODE OF THE CORRESPONDING BEAM. HERE, AND IN FIGS. 7 AND 8, INDIVIDUAL DATA POINTS HAVE BEEN REMOVED FOR CLARITY.

.

SENSOR METRICS

To facilitate comparison between the device presented here and other resonant mass sensor designs, it is prudent to briefly discuss a small number of pertinent sensor metrics. In the case of mass sensors, the most relevant metric is mass sensitivity, that is the smallest change in mass that can be accurately detected using a given sensor. For mass sensors operating in a resonant mode, mass sensitivity is dependent on two independent metrics: mass responsivity and frequency resolution. The mass responsivity of a system is a largely deterministic quantity that dictates how much the resonant frequency of a system changes with a small mass addition. Frequency resolution, on the other hand, quantifies the smallest frequency shift that can be measured in the presence of noise and uncertainty. In general, if frequency shifts are induced primarily through mass addition, the mass sensitivity, ∂m, of a resonant sensor can be approximated by

$$\partial m \approx S^{-1}\partial\omega_0 \tag{11}$$

where S is the mass responsivity and $\partial\omega_0$ is the system's frequency resolution. For the multi-degree-of-freedom sensor detailed here, however, this must be modified to account for N resonance shifts induced by up to N mass changes. This results in a mass sensitivity at the jth microbeam, Δm_j, which is approxi-

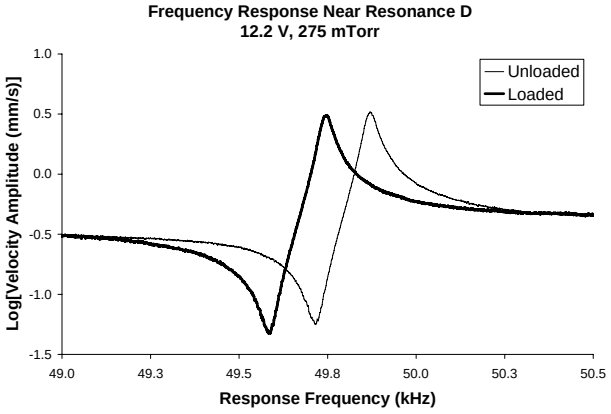

Figure 7. EXPERIMENTALLY-OBTAINED FREQUENCY RESPONSE NEAR RESONANCE (D) FOR THE SENSOR DEPICTED IN FIG. 1 ACTUATED WITH A 12.2 V AC SIGNAL IN 275 mTORR PRESSURE [18]. NOTE THAT THE MASS LOADING INTRODUCES A RESONANCE SHIFT OF 124 Hz.

.

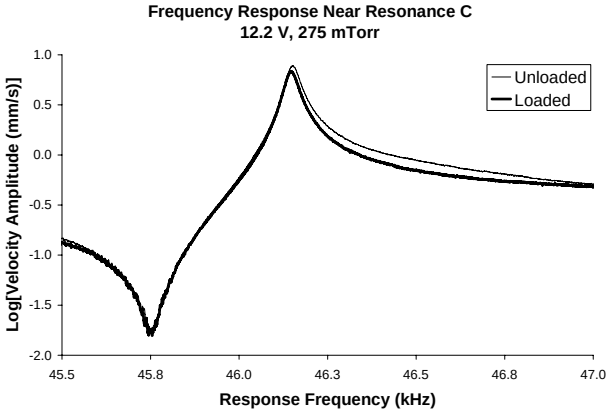

Figure 8. EXPERIMENTALLY-OBTAINED FREQUENCY RESPONSE NEAR RESONANCE (C) FOR THE SENSOR DEPICTED IN FIG. 1 ACTUATED WITH A 12.2 V AC SIGNAL IN 275 mTORR PRESSURE [18]. NOTE THAT THE MASS LOADING INTRODUCES A RESONANCE SHIFT OF 3 Hz.

.

mated by

$$\Delta m_j \approx S_{ij}^{-1}\Delta\omega_i \tag{12}$$

where S_{ij} represents the i,j component of the mass responsivity matrix, which quantifies the shift in ith resonance of the system due to mass addition at the jth oscillator, and $\Delta\omega_i$ quantifies the frequency resolution associated with the ith resonance.

Copyright © 2006 by ASME

Using the experimental results detailed in the previous section the mass responsivity matrix associated with the device shown in Fig. 1 can be partially compiled. For example, the mass responsivity associated with resonance (D) and a mass addition to the highest frequency microbeam can be computed to be 3.3 Hz/pg. Similarly, the mass responsivity associated with resonance (C) and a mass addition to the highest frequency microbeam can be computed to be approximately 0.1 Hz/pg. Continuing with these computations will reveal a diagonally dominant mass responsivity matrix. This can be attributed to the localized nature of the response, which, as detailed in the previous section, leads to significantly larger shifts in the resonances associated with the localized modes of the mass loaded microbeams. It is worth noting that this diagonal structure also ultimately facilitates the simultaneous detection of multiple analytes. For example, in situations where two target analytes are present, the system will exhibit two distinct resonance shifts and a number of comparatively smaller shifts which are a by-product of coupling. Given prior knowledge of the sensor's functionality and the fact that the two resonance shifts associated with the localized modes of the mass-added microbeams are markedly larger, each of the analytes present should be readily identifiable, as was the case with the single 'analyte' (platinum patch) in the preceding section.

Though the experimentally-determined mass responsivities reported above are comparable to other reported values for resonant multi-analyte sensors, they are significantly lower than those reported for sensors based on isolated microresonators [14, 16, 27]. While much of this difference can be rectified through device scaling, it is important to note that the responsivities of the device presented here will always be slightly inferior to those of other microsensors. This can attributed to inter-oscillator coupling, which manifests itself in the off-diagonal terms of the responsivity matrix, which leads to small shifts in each of the system's resonances, not just that associated with the localized mode of the altered beam. Current design studies are aimed at minimizing these off-diagonal terms while still allowing for the detection of resonance shifts using the shuttle mass' response.

Though the impact of thermomechanical noise, temperature fluctuations, adsorption-desorption noise, and other effects known to contribute to a system's frequency resolution have been examined for isolated resonant microsensors (see, for example, [28]), the impact of these effects in coupled oscillator systems has thus far not been considered. Accordingly, present understanding facilitates, at best, a conservative estimate of the frequency resolution(s) associated with the sensor considered herein. For present purposes a frequency resolution of approximately 1 Hz is assumed. This results in a sub-picogram mass sensitivity. Current studies are aimed at extending the results of [28] to multi-degree-of-freedom devices in hopes of refining this approximation.

DESIGN AND INTEGRATION ISSUES

Though a number of design issues have been detailed throughout the course of the present work, it is important to note that there are a number of additional design and integration issues that must be considered in the course of sensor development. The following subsections briefly detail some of most pertinent issues.

Response Measurement

Because it had been predetermined that laser vibrometry would be used to recover the frequency responses detailed in this study, integrated measurement devices were a secondary concern. In implementation, however, the method of response measurement is arguably the most important design consideration. Capacitance changes induced in the electrostatic comb drives included in the original device design could be used to measure the shuttle mass' response, but the magnitudes of these capacitance changes, even near resonance, (approximately 0.4 fF) were insufficient for accurate measurement with off-chip electronics. While it may be possible to detect these changes with on-chip CMOS electronics, future sensor designs would likely benefit from the inclusion of alternative transduction mechanisms. Piezoelectric elements, which transduce strain into voltage, have been successfully integrated in some SDOF microsensors and may be suitable alternatives to the electrostatic comb drives. Likewise, magnetomotive techniques, which have been used to obtain displacement measurements in nanoscale devices and yield response proportional emf voltages, may prove sufficient [29, 30].

Environmental Issues

Though the device examined herein was shown to operate successfully in a partial vacuum environment (275 mTorr), it is important to note that, due to fluid pumping between the microbeams and the sidewalls of the device's substrate, simulated mass detection failed at 1 atm. While mass sensing in partial vacuum may be suitable in some instances, the vast majority of applications will require that the device operate flawlessly in ambient pressures. As such, the next generation of SISO, multi-analyte sensors must be designed to operate in ambient environmental conditions. Device scaling, the removal of excess substrate material, and geometrical reconfiguration of the sensor will likely yield sufficient results at 1 atm. However, if these changes prove insufficient, exploitation of alternative geometries, including in-plane torsional devices, and/or the coupled system's phase response may prove fruitful.

Surface Functionalization

As previously noted, mass addition was realized in this work via the deposition of a small platinum patch on one of the sen-

Copyright © 2006 by ASME

sor's microbeams. In practice, however, resonance shifts typically arise from the accretion of a substance onto a functionalized, chemically-selective surface. In recent years, a considerable amount of research has focused on the development of chemically-active surfaces for use in microcantilever sensors (see, for example, [9, 10, 12, 31, 32]). In the course of sensor development, these prior techniques can be adopted to functionalize cantilever surfaces with different chemicals (metals, polymers, etc.), thus allowing for the detection of multiple analytes using the SISO sensor.

System Integration

A final issue that must be dealt with in the course of sensor design is the integration of the microelectromechanical sensor with integrated or external circuitry capable of measuring resonance shifts in the system's response. Convention presently dictates the use of phase locked loops for such purposes, but it is not readily apparent that such circuits will suffice (or be efficient) for the detection of multiple resonance shifts. Ongoing research is aimed at examining this approach, as well as other candidate techniques, including the post-processing of acquired data using computer algorithms.

CONCLUSION

This work details a preliminary analytical and experimental investigation of a resonant, single input - single output (SISO) microsensor, which exploits vibration localization in a set of coupled, functionalized microbeams to allow for the detection of multiple analytes. In the course of the present work, it was shown that a linear, multi-degree-of-freedom (MDOF), lumped-mass model of the sensor proves sufficient for analysis and predictive design. This model was subsequently used to show N distinct resonance shifts could be detected using solely the response of the sensor's shuttle mass, providing the system was sufficiently localized – a fact which was verified experimentally. Performance metrics of the sensor were also examined. Of particular note is the preliminary design's mass responsivity, the pertinent value of which was determined to be approximately 3.3 Hz/pg – a value comparable to those reported for other multi-analyte resonant sensors, yet inferior to those reported for isolated microresonators.

Though the results of this preliminary investigation validated the SISO, multi-analyte sensor concept, they also revealed a number of issues that must be addressed in future studies. Of these issues, the need for a MDOF frequency resolution model, improved operation in ambient environmental conditions, and robust measurement methods are of particular concern. An ongoing analytical and experimental campaign is aimed at addressing these and other related issues.

ACKNOWLEDGMENT

This work was graciously supported by the National Science Foundation under grant NSF-ECS-0428916.

REFERENCES

[1] Battiston, F. M., Ramseyer, J. P., Lang, H. P., Baller, M. K., Gerber, C., Gimzewski, J. K., Meyer, E., and Guntherodt, H. J., 2001. "A chemical sensor based on a microfabricated cantilever array with simultaneous resonance-frequency and bending readout". *Sensors and Actuators B: Chemical,* **77**(1-2), pp. 122–131.

[2] Davis, Z. J., Abadal, G., Kuhn, O., Hansen, O., Grey, F., and Boisen, A., 2000. "Fabrication and characterization of nanoresonating devices for mass detection". *Journal of Vacuum Science and Technology B,* **18**(2), pp. 612–616.

[3] Ekinci, K. L., Huang, X. M. H., and Roukes, M. L., 2004. "Ultrasensitive nanoelectromechanical mass detection". *Applied Physics Letters,* **84**(22), pp. 4469–4471.

[4] Ilic, B., Czaplewski, D., Craighead, H. G., Neuzil, P., Campagnolo, C., and Batt, C., 2000. "Mechanical resonant immunospecific biological detector". *Applied Physics Letters,* **77**(3), pp. 450–452.

[5] Nugaeva, N., Gfeller, K. Y., Backmann, N., Lang, H. P., Duggelin, M., and Hegner, M., 2005. "Micromechanical cantilever array sensors for selective fungal immobilization and fast growth detection". *Biosensors and Bioelectronics,* **21**(6), pp. 849–856.

[6] Ono, T., Li, X., Miyashita, H., and Esashi, M., 2003. "Mass sensing of adsorbed molecules in sub-picogram sample with ultrathin silicon resonator". *Review of Scientific Instruments,* **74**(3), pp. 1240–1243.

[7] Raiteri, R., Grattarola, M., Butt, H.-J., and Skladal, P., 2001. "Micromechanical cantilever-based biosensors". *Sensors and Actuators B: Chemical,* **79**(2-3), pp. 115–126.

[8] Sharos, L. B., Raman, A., Crittenden, S., and Reifenberger, R., 2004. "Enhanced mass sensing using torsional and lateral resonances in microcantilevers". *Applied Physics Letters,* **84**(23), pp. 4638–4640.

[9] Su, M., Li, S., and Dravid, V. P., 2003. "Microcantilever resonance-based DNA detection with nanoparticle probes". *Applied Physics Letters,* **82**(20), pp. 3562–3564.

[10] Thundat, T., Wachter, E. A., Sharp, S. L., and Warmack, R. J., 1995. "Detection of mercury vapor using resonating microcantilevers". *Applied Physics Letters,* **66**(13), pp. 1695–1697.

[11] Zribi, A., Knobloch, A., Tian, W.-C., and Goodwin, S., 2005. "Micromachined resonant multiple gas sensor". *Sensors and Actuators A: Physical,* **122**(1), pp. 31–38.

[12] Lang, H. P., Berger, R., Battiston, F., Ramseyer, J.-P., Meyer, E., Andreoli, C., Brugger, J., Vettiger, P., Despont, M., Mezzacasa, T., Scandella, L., Guntherodt, H.-J., Ger-

Copyright © 2006 by ASME

ber, C., and Gimzewski, J. K., 1998. "A chemical sensor based on a micromechanical cantilever array for the identification of gases and vapors". *Applied Physics A: Material Science & Processing,* **66**(Supplement 1), pp. S61–S64.

[13] Gfeller, K. Y., Nugaeva, N., and Hegner, M., 2005. "Micromechanical oscillators as rapid biosensor for the detection of active growth of escherichia coli". *Biosensors and Bioelectronics,* **21**(3), pp. 528–533.

[14] Yang, Y. T., Callegari, C., Feng, X. L., Ekinci, K. L., and Roukes, M. L., 2006. "Zeptogram-scale nanomechanical mass sensing". *Nano Letters,* **6**(4), pp. 583–586.

[15] Chen, G. Y., Thundat, T., Wachter, E. A., and Warmack, R. J., 1995. "Adsorption-induced surface stress and its effects on resonance frequency of microcantilevers". *Journal of Applied Physics,* **77**(6), pp. 3618–3622.

[16] Lang, H. P., Hegner, M., and Gerber, C., 2005. "Cantilever array sensors". *Materials Today,* **8**(4), pp. 30–36.

[17] Ren, Q., and Zhao, Y.-P., 2004. "Influence of surface stress on frequency of microcantilever-based biosensors". *Microsystem Technologies,* **10**(4), pp. 307–314.

[18] DeMartini, B. E., Rhoads, J. F., Shaw, S. W., and Turner, K. L., 2006. "A resonant SISO sensor based on a coupled array of microelectromechanical oscillators". Proceedings of Hilton Head 2006: A Solid-State Sensor, Actuator, and Microsystems Workshop.

[19] Maidanik, G., and Becker, K. J., 1998. "Noise control of a master harmonic oscillator coupled to a set of satellite harmonic oscillators". *Journal of the Acoustical Society of America,* **104**(5), pp. 2628–2637.

[20] Xu, K., and Igusa, T., 1992. "Dynamic characteristics of multiple substructures with closely spaced frequencies". *Earthquake Engineering and Structural Dynamics,* **21**(12), pp. 1059–1070.

[21] Weaver, R. L., 1997. "Mean and mean-square responses of a prototypical master/fuzzy structure". *Journal of the Acousitcal Society of America,* **101**(3), pp. 1441–1449.

[22] Meirovitch, L., 1986. *Elements of Vibration Analysis*, 2nd ed. McGraw-Hill, New York.

[23] Pierre, C., and Dowell, E. H., 1987. "Localization of vibrations by structural irregularity". *Journal of Sound and Vibration,* **114**(3), pp. 549–564.

[24] Zhang, W., Zhang, W., Turner, K., and Hartwell, P. G., 2004. "SCREAM'03: A single mask process for high-Q single crystal silicon MEMS". Proceedings of the 2004 ASME International Mechanical Engineering Congress and Exposition, IMECE2004-61140.

[25] Turner, K. L., Hartwell, P. G., and MacDonald, N. C., 1999. "Multi-dimensional MEMS motion characterization using laser vibrometry". Proceedings of Transducers '99: The 10th International Conference on Solid-state Sensors and Actuators, pp. 1144–1147.

[26] Dohn, S., Sandberg, R., Svendsen, W., and Boisen, A., 2005. "Enhanced functionality of cantilever based mass sensors using higher modes". *Applied Physics Letters,* **86**, 233501.

[27] Ilic, B., Czaplewski, D., Zalalutdinov, M., Craighead, H. G., Neuzil, P., Campagnolo, C., and Batt, C., 2001. "Single cell detection with micromechanical oscillators". *Journal of Vacuum Science and Technology B,* **19**(6), pp. 2825–2828.

[28] Ekinci, K. L., Yang, Y. T., and Roukes, M. L., 2004. "Ultimate limits to inertial mass sensing based upon nanoelectromechanical systems". *Journal of Applied Physics,* **95**(5), pp. 2682–2689.

[29] Cleland, A. N., 2003. *Foundations of Nanomechanics: From Solid-State Theory to Device Applications*. Advanced Texts in Physics. Springer, Berlin.

[30] Mohanty, P., Harrington, D. A., Ekinci, K. L., Yang, Y. T., Murphy, M. J., and Roukes, M. L., 2002. "Intrinsic dissipation in high-frequency micromechanical resonators". *Physical Review B,* **66**, 085416.

[31] Lang, H. P., Berger, R., Andreoli, C., Brugger, J., Despont, M., Vettiger, P., Gerber, C., Ramseyer, J. P., Meyer, E., and Guntherodt, H.-J., 1998. "Sequential position readout from arrays of micromechanical cantilever sensors". *Applied Physics Letters,* **72**(3), pp. 383–385.

[32] Thundat, T., Chen, G. Y., Warmack, R. J., Allison, D. P., and Wachter, E. A., 1995. "Vapor detection using resonating microcantilevers". *Analytical Chemistry,* **67**(3), pp. 519–521.

Copyright © 2006 by ASME